Supporting Information

Atomic-Scale Visualization of Single Atom Formation in Metal-Organic Frameworks

Kai-Yuan Hsiao,[a] Yi-Dong Lin,[a] Yu-Ru Lin,[a] Ching-Wei Chin,[d] Chun-Hui Lin,[a] Ruei-Hong Cyu,[a] Yan-Gu Lin,[bc] Yu-Lun Chueh,[adef] and Ming-Yen Lu*[ad]

[a]Department of Materials Science and Engineering, National Tsing Hua University, Hsinchu 300, Taiwan

[b]Scientific Research Division, National Synchrotron Radiation Research Center, Hsinchu 300092, Taiwan

[c]Department of Materials Science and Engineering, National Yang-Ming Chiao Tung University, Hsinchu 300093, Taiwan

[d]College of Semiconductor Research, National Tsing Hua University, Hsinchu 30013, Taiwan

[e]Department of Physics, National Sun Yat-Sen University, Kaohsiung 80424, Taiwan

[f]Department of Materials Science and Engineering, Korea University, Seoul 02841, Republic of Korea

*E-mail: mylu@mx.nthu.edu.tw

Experimental Section

Synthesis of Fe-ZIF

$Zn(NO_3)_2$ (0.5904 g) and 2-methylimidazole (2-mIM, 1.3020 g) were dissolved individually in MeOH (20 mL) under sonication. Then, $Fe(acac)_3$ (0.07 g) were added to $Zn(NO_3)_2$ solution under sonication. The solutions of 2-mIM and $Zn(NO_3)_2$ solution were mixed and stirred for 5 min, followed by placing at room temperature (RT) for 12 h. The resulting precipitation was collected, washed with MeOH (at least three times), and dried at 80 °C for 12 h.

Synthesis of Fe-400, Fe-900, and Fe-1100

The ZIF-8 powders were placed in Al_2O_3 crucibles, loaded into a tube furnace, heated to 400 °C, 900 °C and 1100 °C (at 5 °C/min) under an Ar flow and held for 3 h, for Fe-400, Fe-900, and Fe-1100, respectively. Then, the furnaced was cooled to RT naturally.

Material Characterization

The morphologies, compositions, and phases of the materials were investigated using scanning electron microscopy (SEM, Hitachi SU8010), X-ray diffractometry (XRD, Bruker D2 phaser) with Cu Kα radiation, and high-resolution X-ray photoelectron spectrometry (HR-XPS, ULVAC-PHI PHI 5000 Versaprobe II). TEM and scanning

TEM (STEM) images were recorded using a spherical-aberration-corrected field-emission transmission electron microscope (Cs-corrected TEM, JEOL ARM-200FTH) at an accelerating voltage of 200 kV. Elemental distributions were measured using equipped energy dispersive spectrometry (EDS).

In situ STEM observation

In situ STEM observation was performed using the JEOL ARM-200FTH microscope operated at 200 kV. The Fe-ZIF particles were dispersed in EtOH. A drop of the resulting solution was placed on a dedicated E-chip and dried at 60 °C. The E-chip was assembled in an in situ heating holder (Fusion, Protochips). To minimize the effect of electron beam irradiation, the current density was maintained below 16 pA/cm^2.

Computational method

The density functional theory (DFT) calculations were utilized the Vienna ab initio simulation package (VASP) with plane-wave basis sets and the projector augmented-wave (PAW) method.[1-4] The exchange-correlation potential followed the generalized gradient approximation (GGA) using the Perdew-Burke-Ernzerhof (PBE) parametrization,[5] supplemented by Grimme's DFT-D3 model for van der Waals corrections.[6] A cutoff energy of 520 eV and a Γ-centered Monkhorst-Pack mesh of 2 × 2 × 1 were employed for Brillouin-zone integration.[7] In cases involving strongly correlated Fe atoms, a spin-polarized DFT+U correction with U = 5.3 eV was applied. Structural relaxation continued until forces on each atom were less than 0.01 eV/Å, achieving an energy convergence threshold of 10^{-5} eV. Optimization ensured structures reached their minimum energy states. To ascertain optimized diffusion paths of

[Fe(acac)]$^{2+}$ molecules (with one and three) on surfaces, the climbing-image nudged elastic band (CI-NEB) method utilized seven images per calculation.[8]

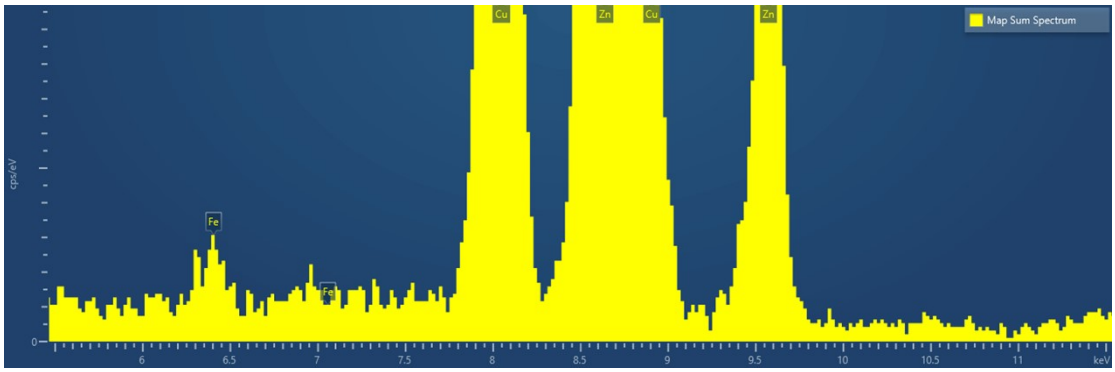

Figure S1. EDS spectrum of Fe-ZIF confirms the successful encapsulation of Fe species within the ZIF framework.

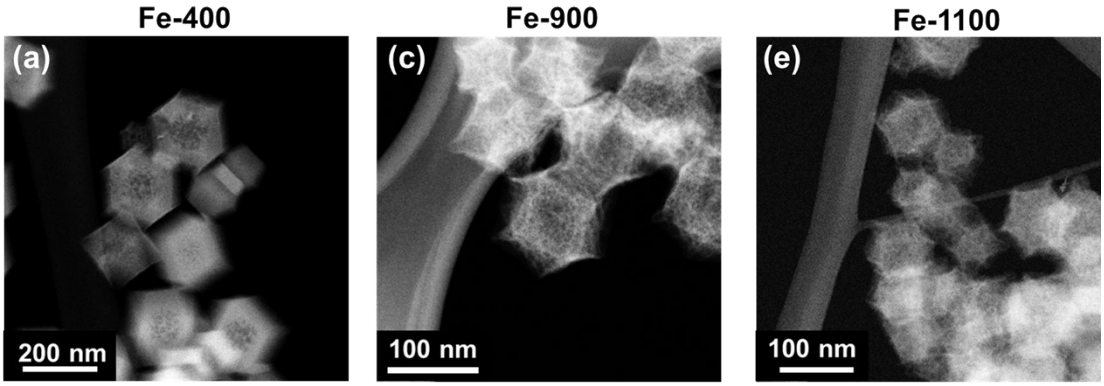

Figure S2. HAADF-STEM images of (a) Fe-400, (b) Fe-900, and (c) Fe-1100.

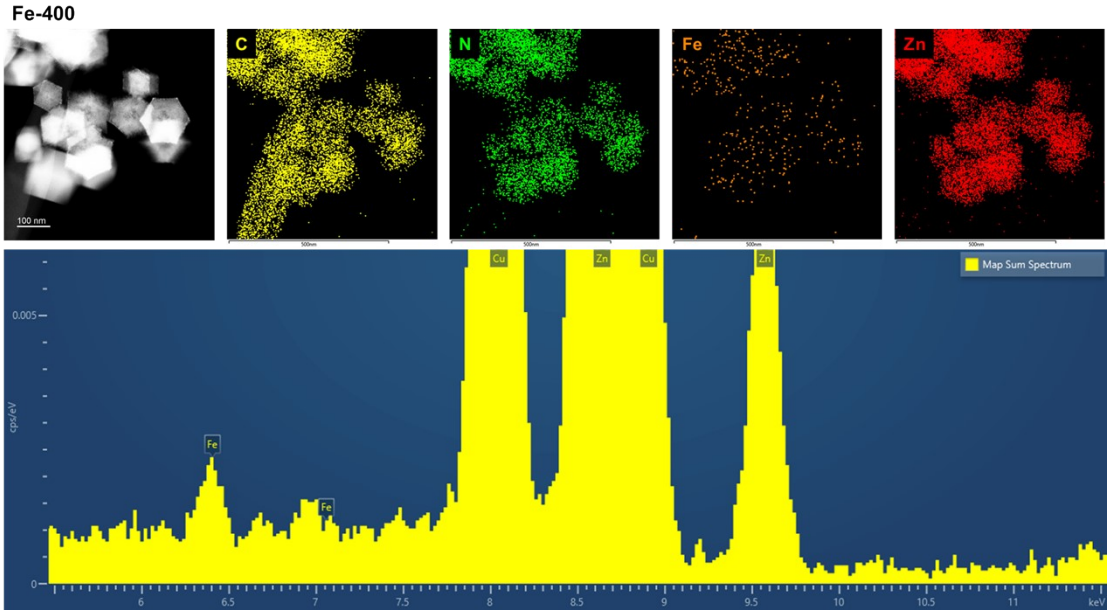

Figure S3. EDS elemental mapping and corresponding spectrum of Fe-400.

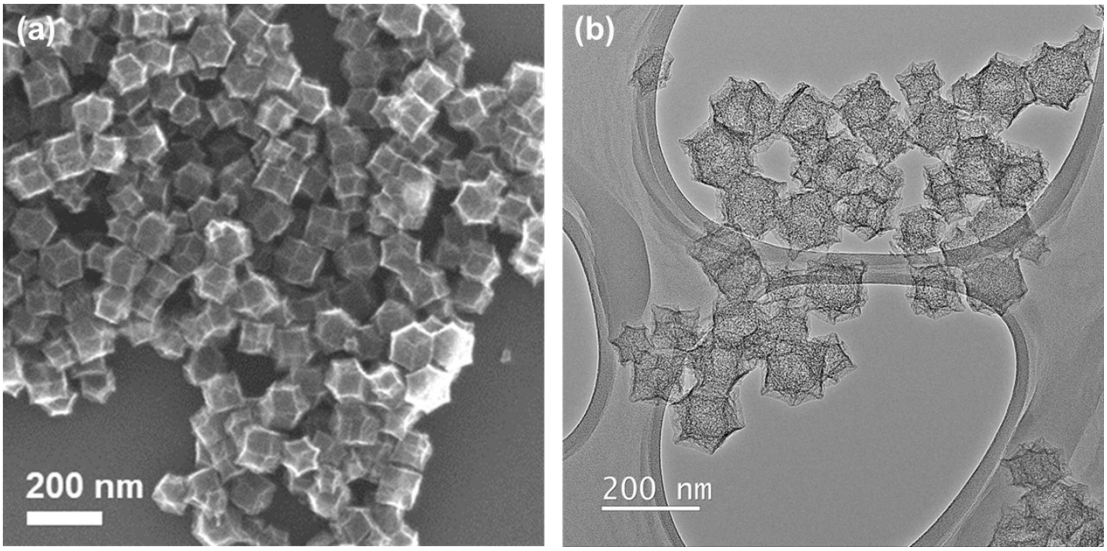

Figure S4. (a) SEM image, **(b)** TEM image Fe-900.

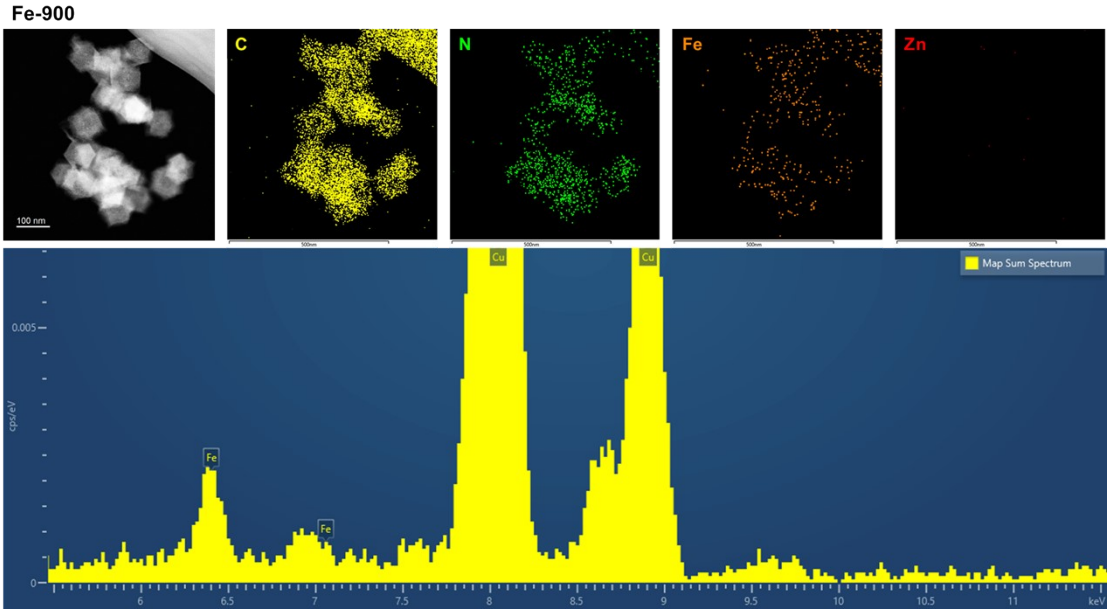

Figure S5. EDS elemental mapping and corresponding spectrum of Fe-900.

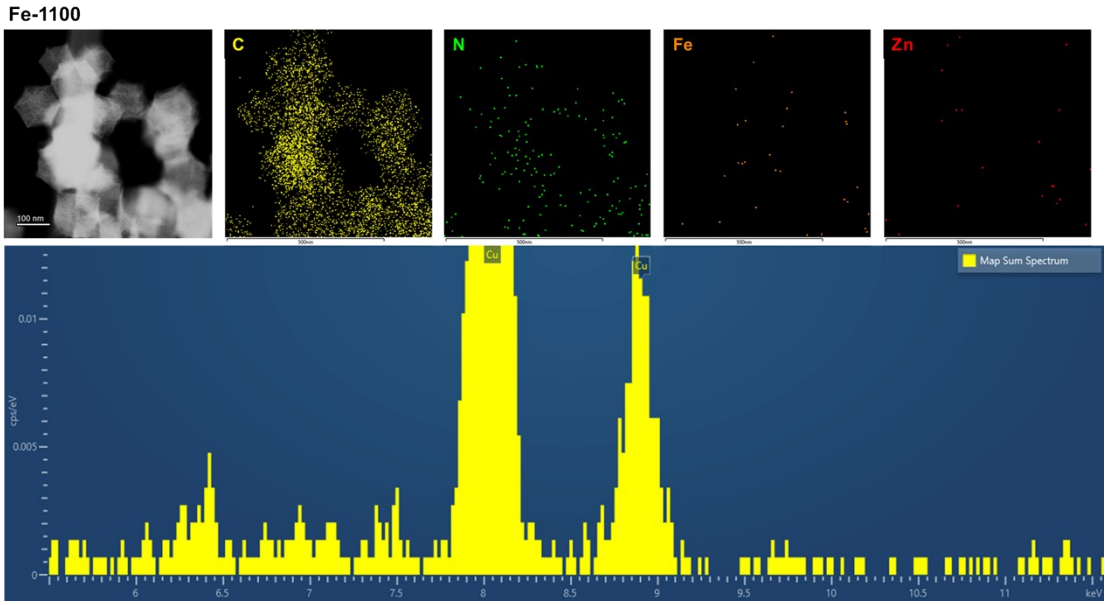

Figure S6. EDS elemental mapping and corresponding spectrum of Fe-1100.

Table S1 Atomic percentages of C, N, Zn, and Fe, as determined by EDS.

	Fe-ZIF	**Fe-400**	**Fe-900**	**Fe-1100**
C	66.4%	73.5%	94.2%	97.3%
N	23.2%	21.9%	5.7%	2.7%
Zn	10.3%	4.5%	0.0%	0.0%
Fe	0.1%	0.1%	0.1%	0.0%

Table S2 The ratios of N and C content of the samples from EDS and XPS.

	N/C (EDS)	N/C (XPS)
Fe-ZIF	0.349	0.399
Fe-400	0.298	0.387
Fe-900	0.061	0.043
Fe-1100	0.028	0.014

Table S3 The Fe content of the samples from XPS analysis.

	Fe content (At %)
Fe-ZIF	0.25
Fe-400	0.39
Fe-900	3.58
Fe-1100	0.02

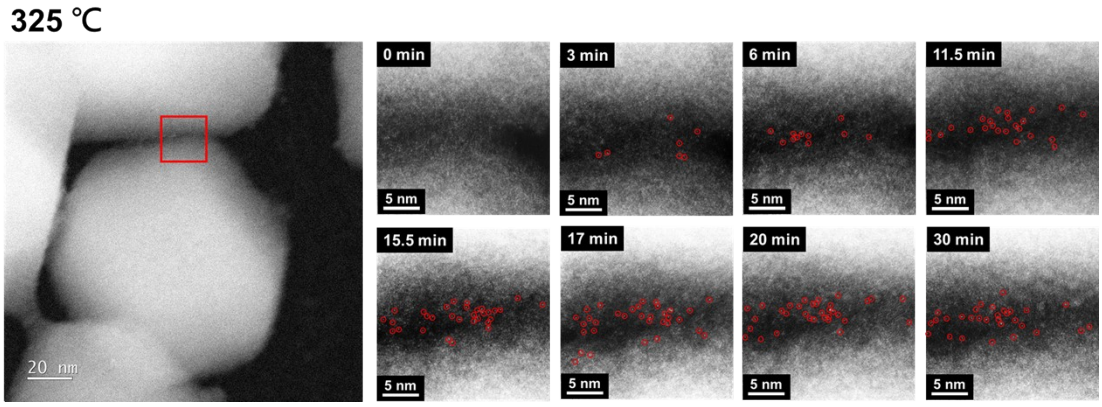

Figure S7. Time-sequenced in situ STEM images of the single atom formation during pyrolysis at 325 ºC for 30 minutes.

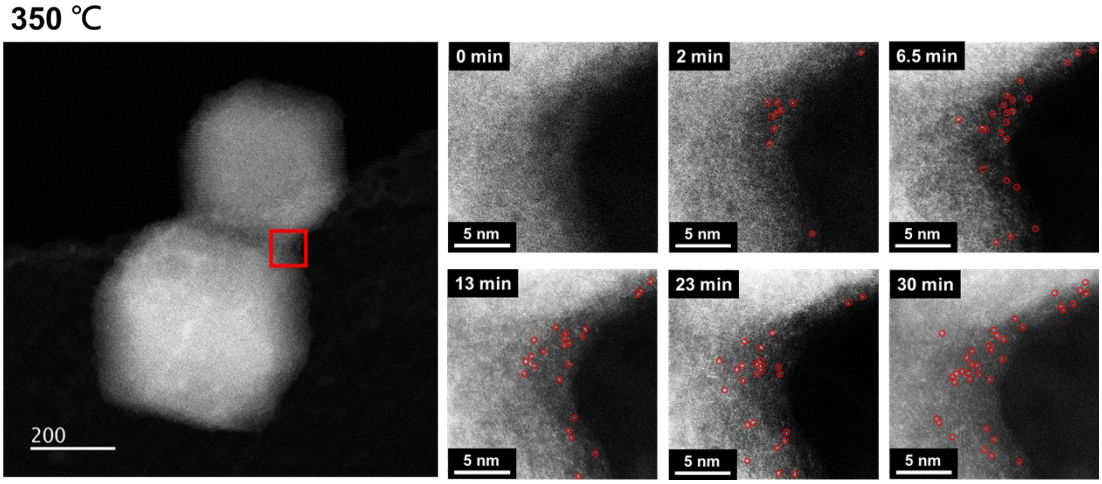

Figure S8. Time-sequenced in situ STEM images of the single atom formation during pyrolysis at 350 ºC for 30 minutes.

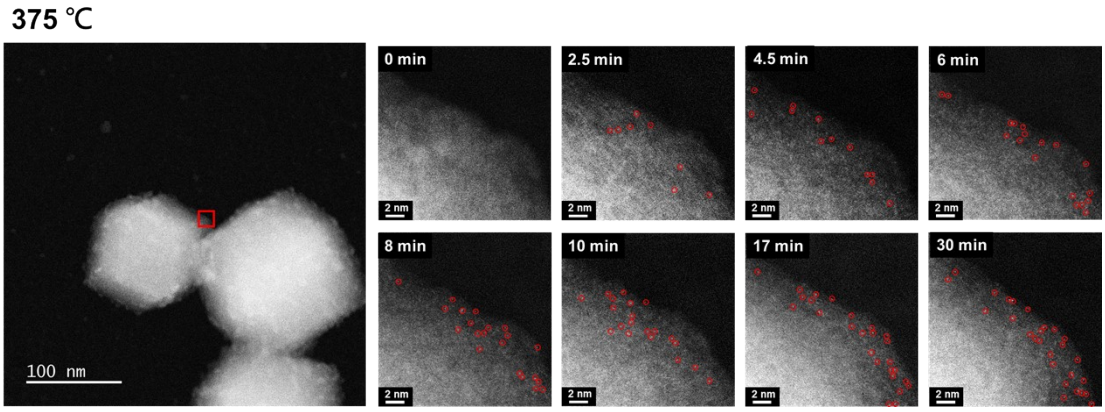

Figure S9. Time-sequenced in situ STEM images of the single atom formation during pyrolysis at 375 ºC for 30 minutes.

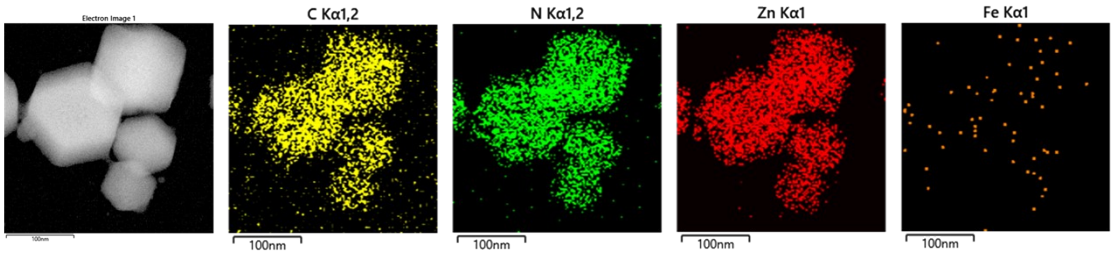

Figure S10. EDS elemental mappings of C, N, Zn, and Fe after pyrolysis at 325 ^{o}C.

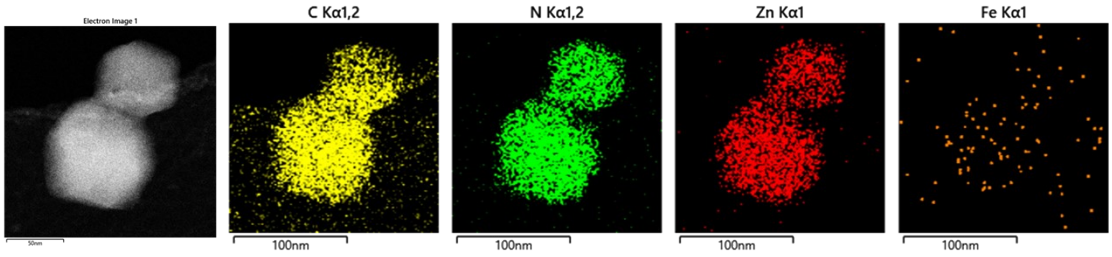

Figure S11. EDS elemental mappings of C, N, Zn, and Fe after pyrolysis at 350 °C.

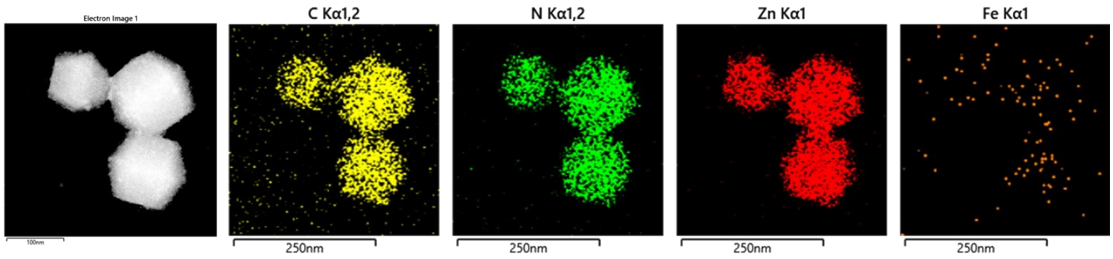

Figure S12. EDS elemental mappings of C, N, Zn, and Fe after pyrolysis at 375 °C.

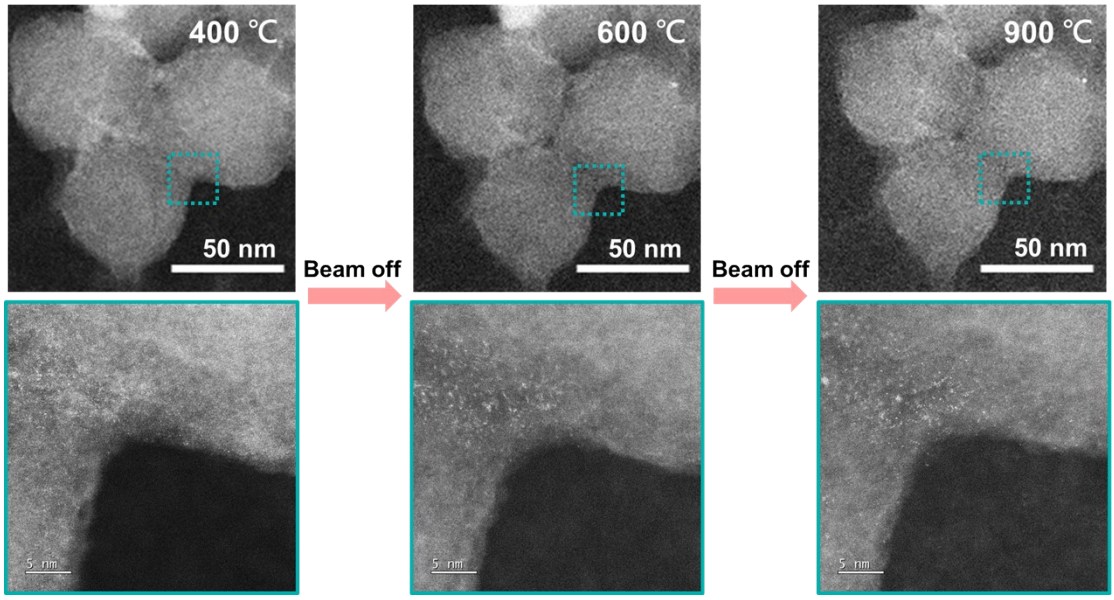

Figure S13. In situ STEM images during pyrolysis without beam irradiation effect.

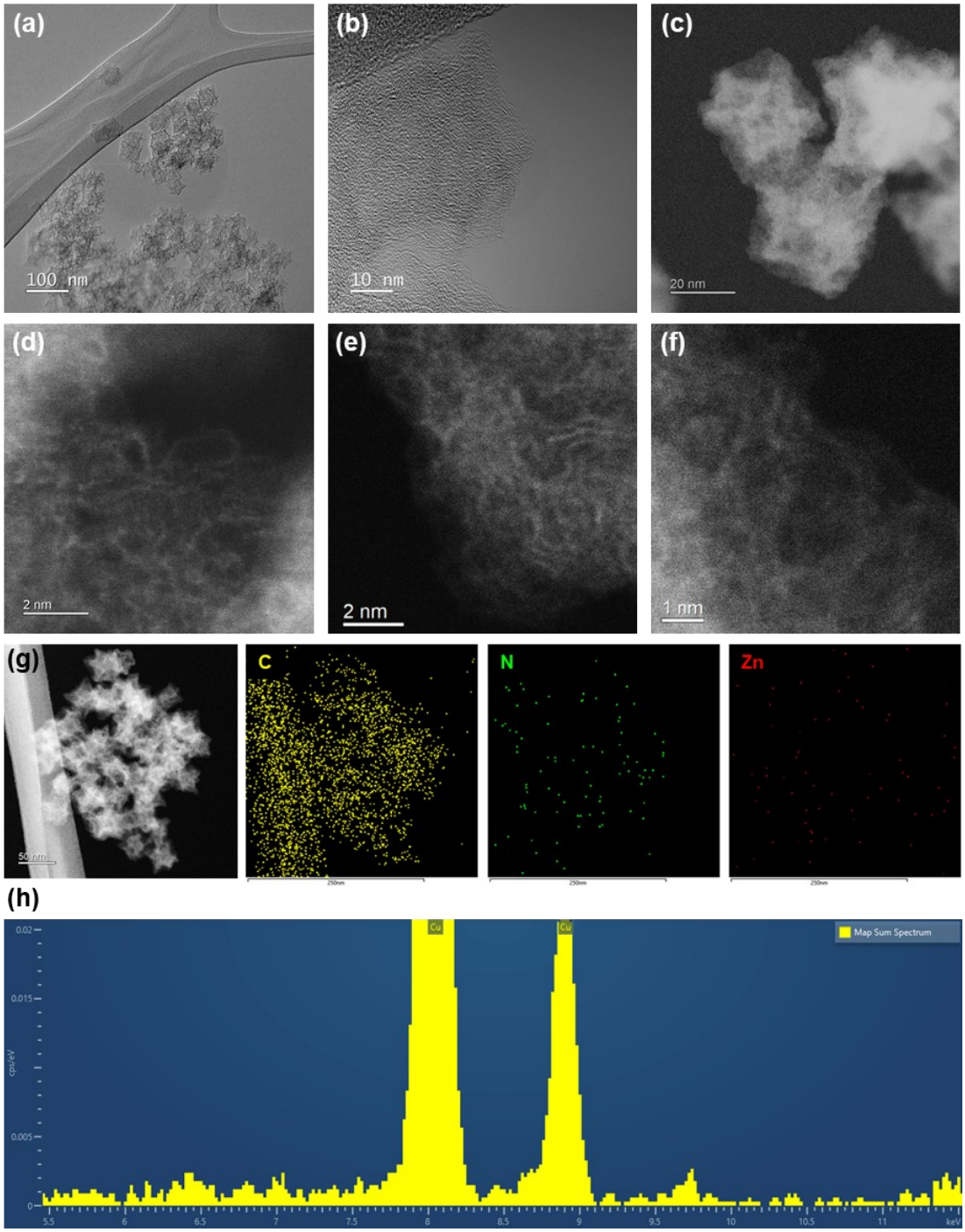

Figure S14. (a) TEM image, **(b)** high-resolution (HR)TEM image, **(c)** HAADF-STEM image, **(d-f)** HR HADDF-STEM images, and **(e)** EDS elemental mappings and **(h)** the corresponding spectrum of the pristine ZIF-8 derived samples after pyrolysis at 900 °C. The results confirm that Zn species were completely evaporated after pyrolysis at 900 °C and no SA is observed in the carbon matrix.

Table S4 k_1 and k_2 value at various pyrolysis temperatures.

	$\mathbf{k_1}$ ($\mu m^{-2} \cdot min^{-1}$)	$\mathbf{k_2}$ ($\mu m^{-2} \cdot min^{-1}$)
400 °C	68027	7608
375 °C	26263	3529
350 °C	18247	1560
325 °C	7177	815

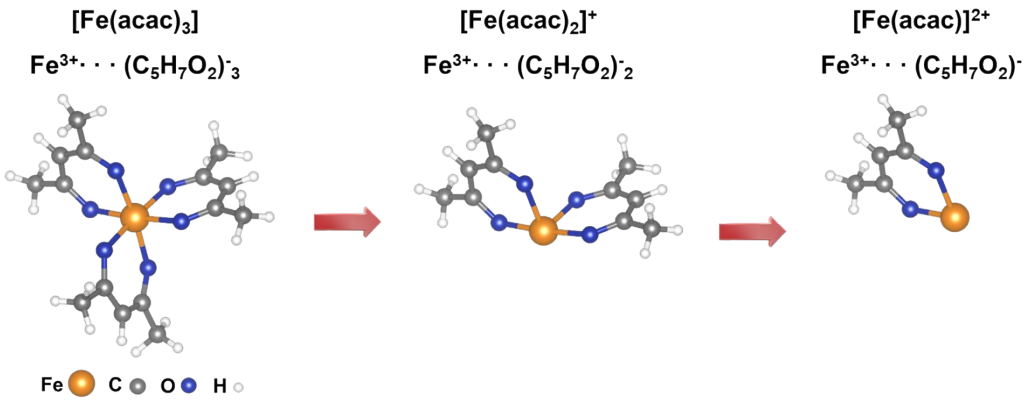

Figure S15. Schematic diagram of the decomposition process of $Fe(acac)_3$ at elevated temperatures.

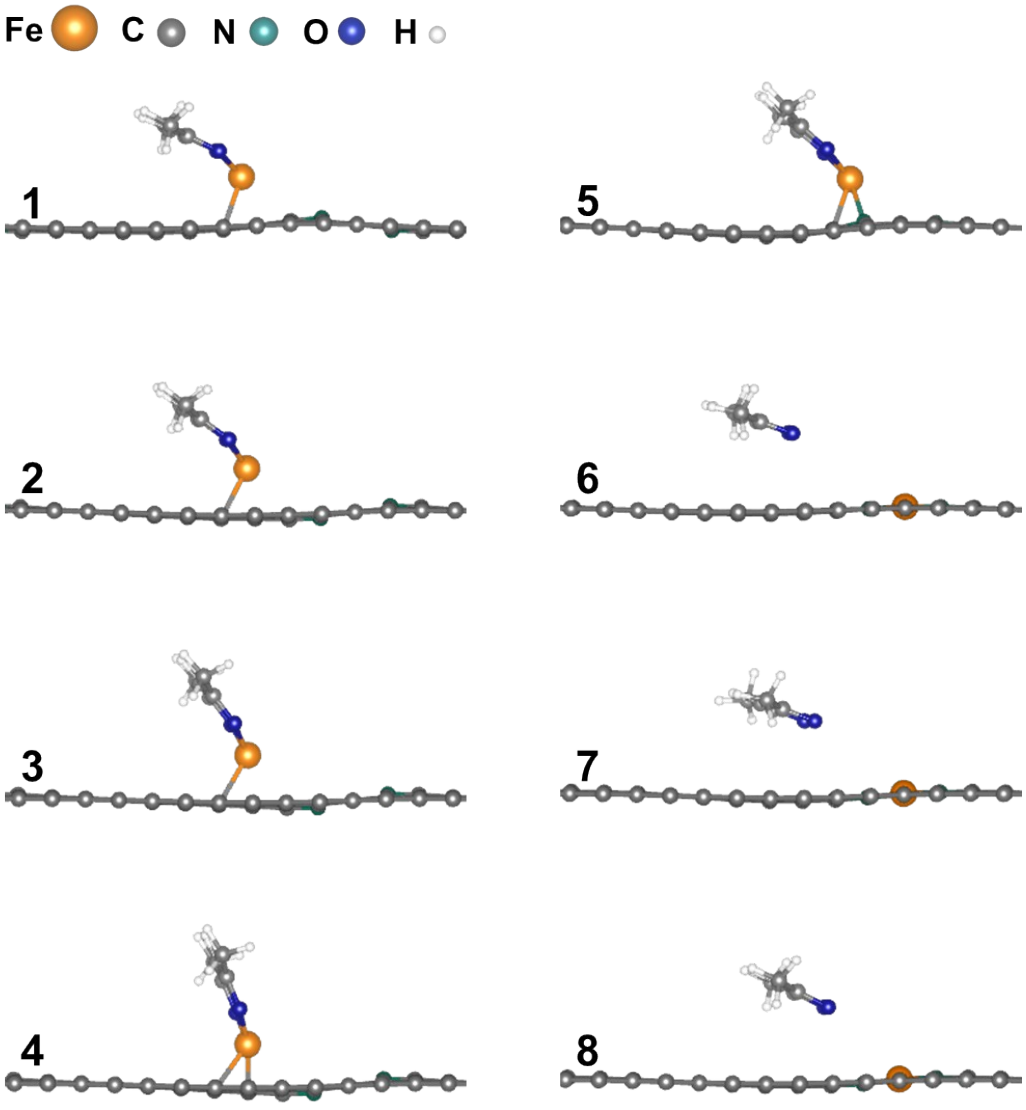

Figure S16. Side view of the atomic structure illustrated the atomization pathway for dispersed $[Fe(acac)]^{2+}$.

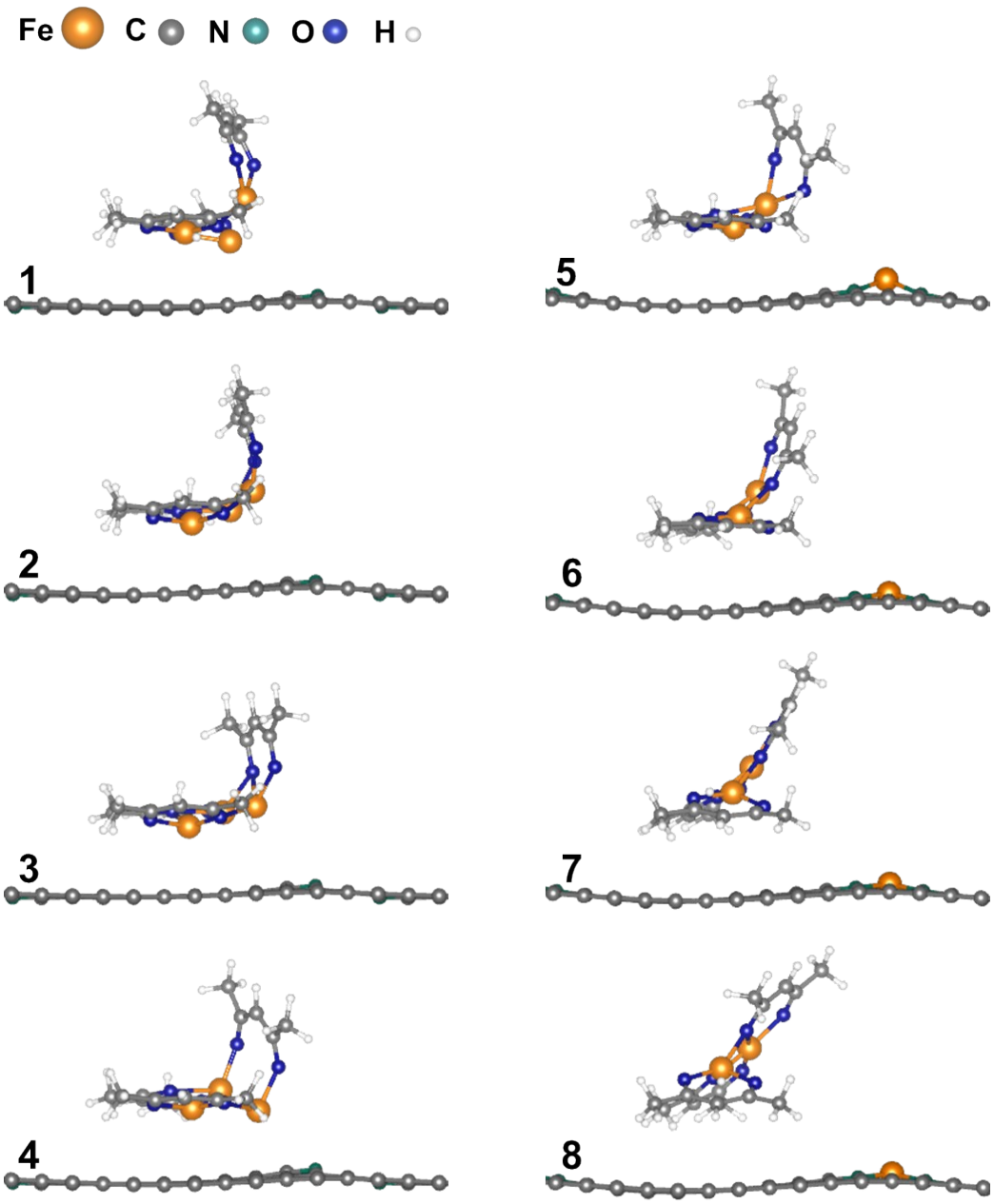

Figure S17. Side view of the atomic structure illustrated the atomization pathway for clustered $[Fe(acac)]^{2+}$.

Reference

1. G. Kresse and J. Furthmüller, *Physical review B*, 1996, **54**, 11169.
2. P. E. Blochl, *Physical Review-Section B-Condensed Matter*, 1994, **50**, 17953-17979.
3. W. Kohn and L. J. Sham, *Phys. Rev.*, 1965, **140**, A1133.
4. P. Hohenberg and W. Kohn, *Phys. Rev*, 1964, **136**, B864.
5. J. P. Perdew, K. Burke and M. Ernzerhof, *Phys. Rev. Lett.*, 1996, **77**, 3865.
6. S. Grimme, J. Antony, S. Ehrlich and H. Krieg, *The Journal of chemical physics*, 2010, **132**.
7. H. J. Monkhorst and J. D. Pack, *Physical review B*, 1976, **13**, 5188.
8. G. Henkelman, B. P. Uberuaga and H. Jónsson, *The Journal of chemical physics*, 2000, **113**, 9901-9904.